RSC Applied Polymers

ROYAL SOCIETY OF CHEMISTRY

PAPER

View Article Online
View Journal



Cite this: DOI: 10.1039/d6lp00051g

# 3D printable polylactone/2-hydroxylethyl acrylate networks with adjustable post-printing mechanical properties

Bo Li,[a,b] Gianluca Bartolini Torres,[a,c] Na Zhao,[d,e] Jonathan J. P. Peters,[f] Guonan Ji,[a,g] Quinten Thijssen [h] and Andreas Heise *[a,b,c]

Photopolymerisation-based 3D printing of biocompatible materials enables the fabrication of highly accurate, customised scaffolds; however, the resulting covalently crosslinked networks typically exhibit fixed mechanical properties. Here, we introduce 3D-printed polyester/acrylate hydrogels with adjustable mechanical properties enabled by chemically orthogonal controlled dual crosslinking. The resin formulation consists of a tetra-cinnamic-acid-functionalised copolyester, poly(caprolactone-*co*-valerolactone) (P(CL-*co*-VL)-CA), blended with 2-hydroxyethyl acrylate (HEA) and the radical crosslinker pentaerythritol tetraacrylate (PETA). Owing to the significantly faster photoreactivity of the acrylate groups, printing proceeds *via* HEA radical polymerisation to form a soft primary network while preserving pendant cinnamic acid functionalities. A secondary network is subsequently introduced through UV-induced [2 + 2] cycloaddition of the cinnamate groups during post-curing. By controlling the post-printing light exposure time, the extent of P(CL-*co*-VL)-CA crosslinking, and hence the elastic modulus of the resulting double-network scaffolds, can be tuned from 0.3 to 1.8 MPa without altering the printed dimensions. Both single- and double-crosslinked P(CL-*co*-VL)-CA/HEA hydrogels supported high levels of cell proliferation. This work demonstrates a versatile strategy for generating mechanically adaptable 3D objects from a single resin formulation through post-printing modulation.

Received 11th February 2026,
Accepted 8th May 2026

DOI: 10.1039/d6lp00051g

rsc.li/rscapplpolym



## Introduction

Supporting the repair of native tissues using biological substitutes has emerged as a promising strategy, known as tissue engineering.[1,2] A key requirement in this process is the fabrication of scaffold materials that reproduce the geometry and mechanical properties of the targeted tissues.[3] 3D printing of photocurable monomers and polymers has become an efficient technology for producing customised tissue engineering scaffolds as it enables rapid fabrication with high spatial accuracy.[4–6] However, covalent networks derived from photopolymerisation typically possess fixed mechanical properties. Systems allowing post-printing modulation of scaffold mechanical properties, including the design of gradient properties, are highly desirable to adapt to the selected cell type and biological environment.[7,8] While several printing approaches have been developed, materials with post-printing tunability remain rare due to their covalent networks. Most examples demonstrate geometric adaptability in response to pH or thermal changes, often referred to as 4D materials.[9–13] However, mechanically adaptable 3D-printed systems remain underexplored. Most reported examples offer only binary mechanical states. For instance, thermal esterification can substantially increase the crosslink density of an acrylate network, thereby enabling reprogramming of its mechanical properties.[14] A double-network approach combining stiff and flexible polymers has also been described, in which stiff thermoplastics are printed *via* radical polymerisation of acrylates, followed by ring-opening polymerisation of lipoic acid to introduce flexibility post-printing.[15] These strategies represent

[a]*Department of Chemistry, RCSI University of Medicine and Health Sciences, Dublin, D02 YN77, Ireland. E-mail: andreasheise@rcsi.ie*
[b]*AMBER, The Research Ireland Advanced Materials and Bioengineering Research Centre, RCSI, Dublin, D02 YN77, Ireland*
[c]*Research Ireland Centre for Research in Medical Devices (CURAM), RCSI, Dublin, D02 YN77, Ireland*
[d]*Tissue Engineering Research Group (TERG), Department of Anatomy and Regenerative Medicine, RCSI University of Medicine and Health Sciences, Dublin 2, Ireland*
[e]*College of Pharmaceutical Sciences, Soochow University, Suzhou 215123, China*
[f]*School of Physics, Trinity College Dublin, College Green, Dublin D02 PN40, Ireland*
[g]*Institute of Functional Nano and Soft Materials (FUNSOM), Collaborative Innovation Center of Suzhou Nano Science and Technology, Soochow University, Suzhou 215123, China*
[h]*Polymer Chemistry and Biomaterials Group, Centre of Macromolecular Chemistry, Department of Organic and Macromolecular Chemistry, Ghent University, Krijgslaan 291 S4, Ghent, 9000 Belgium*

important steps toward overcoming the mechanical limitations of current 3D-printed biomaterials. However, they typically permit only a direct transition between soft and hard states.

Owing to their biocompatibility and biodegradability, aliphatic polyesters, particularly polycaprolactone (PCL), have been widely investigated as materials for 3D printing in tissue engineering[16–19] At physiological temperature, PCL is in a crystalline state and therefore exhibits relatively limited elasticity.[20] Copolymerisation of caprolactone with other monomers such as lactide and δ-valerolactone have therefore been introduced to adjust the crystallinity, further resulting in optimised mechanical properties. Hybrid networks have also proven effective in tuning the thermomechanical properties of polyester-based materials. For example, tough networks have been developed by combining PCL with high glass transition temperature ($T_g$) acrylate monomers, where varying the PCL-to-acrylate ratio enables control over mechanical behaviour.[21] Similarly, flexible networks with distinct stress–strain responses can be produced by blending PCL with low-$T_g$ 2-hydroxy acrylates.[22] Nevertheless, none of these strategies were able to provide tuneable properties post-printing due to their covalent bonds.

In this work, we demonstrate tuneable mechanical properties in 3D-printed polyester-acrylate resins by exploiting chemically controlled dual crosslinking. The formulation comprises a tetra-cinnamic acid-functionalised copolyester, poly(caprolactone-*co*-valerolactone) (P(CL-*co*-VL)-CA), blended with 2-hydroxyethyl acrylate (HEA) and the radical crosslinker pentaerythritol tetraacrylate (PETA) (Fig. 1, $t_0$). Owing to the distinctly faster photoreactivity of the acrylate moieties, the resin can be rapidly cured *via* radical polymerisation of HEA, yielding a soft primary network while preserving pendant cinnamic acid moieties (Fig. 1, $t_1$). A secondary network is subsequently formed through UV-induced [2 + 2] cycloaddition of the cinnamic acid groups during post-curing (Fig. 1, $t_2 - t_n$). We hypothesised that controlling the post-printing irradiation time governing the slower secondary crosslinking process would enable systematic tuning of the mechanical properties as a function of post-curing time.

## Experimental section

### Materials and methods

**Materials.** ε-Caprolactone, δ-valerolactone, and Sudan I were purchased from Tokyo Chemical Industry. Tin(II) octoate, cinnamic acid, pentaerythritol, 2-hydroxyethyl acrylate, pentaerythritol tetraacrylate (PETA), phenylbis(2,4,6-trimethylbenzoyl) phosphine oxide (BAPO), benzophenone and 2,2,6,6-tetramethylpiperidine 1-oxyl (TEMPO) were purchased from Sigma Aldrich.

**Synthesis of poly(valerolactone-*co*-caprolactone)-cinnamic acid.** Poly(valerolactone-*co*-caprolactone) was synthesized *via* ring-opening polymerization of ε-caprolactone (17.1 g, 150 mmol, 12 eq.) and δ-valerolactone (10.0 g, 100 mmol, 8 eq.) using pentaerythritol (1.7 g, 12.5 mmol, 1 eq.) as an initiator and tin(II) octoate (120 mg, 0.296 mmol, 0.02 eq.) as a catalyst. The reaction mixture was stirred under a nitrogen atmosphere at 110 °C for 16 hours. Subsequently, cinnamic acid (7.4 g, 50 mmol, 4 eq.) was added into the reaction mixture, followed by stirring under nitrogen at 130 °C for 5 days. The polymer was used without purification.

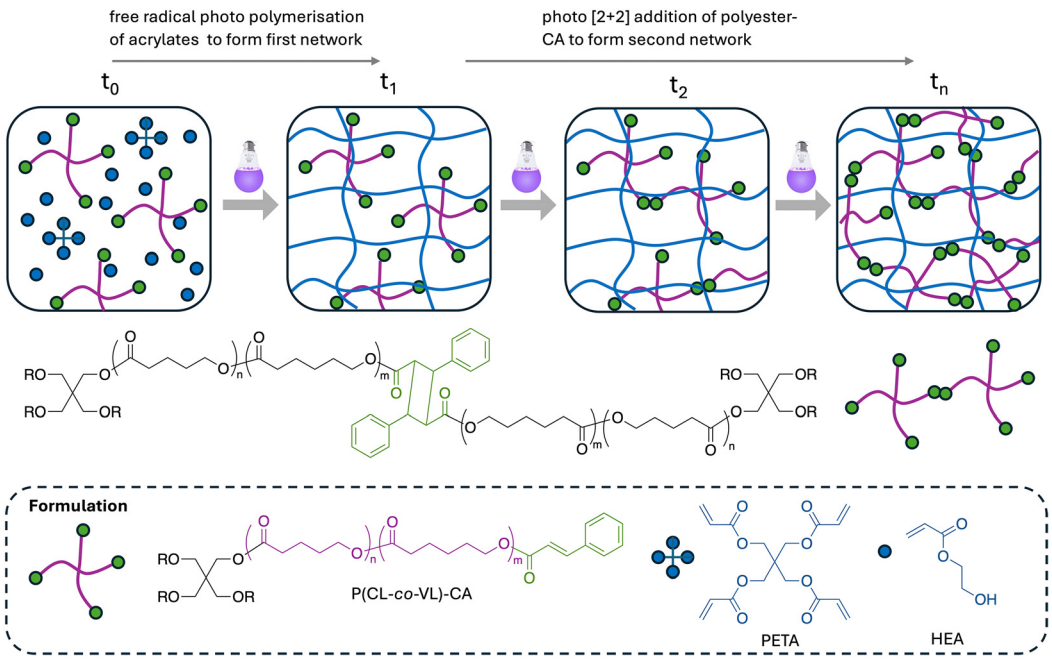


**Fig. 1** Conceptual approach to 3D printable mechanically tuneable dual networks. Formulation: poly(valerolactone-*co*-caprolactone), (PCL-*co*-VL)-CA, hydroxyethyl acrylate (HEA), pentaerythritol tetraacrylate (PETA), phenylbis(2,4,6-trimethylbenzoyl)phosphine oxide (BAPO, not shown).

**Sample preparation for swelling and tensile test.** The resins were poured into rectangular molds ($H$0.8 × $W$10 × $L$20 mm) and irradiated with UV light of 405 nm (9 mW cm$^{-2}$) for 2 min at room temperature. Afterward, the cross-linked sheets were post-cured for the desired time under 365 nm UV light (9 mW cm$^{-2}$).

**Swelling test.** The Gel fraction and swelling ratio were calculated on cross-linked sheets prepared as described. The cross-linked sheets were weighed (initial dry mass $W_d$). Then they were immersed in excess acetone for 48 h at room temperature, and then weighed again to obtain the swollen mass ($W_s$). Next, the swollen samples were dried in a vacuum oven (40 °C) overnight to measure the dry mass after swelling ($W_a$). Using the following equations, the gel fraction and swelling ratio were calculated. All the measurements were performed in triplicate.

$$\text{Gel fraction}\,(\%) = \frac{W_a}{W_d} \times 100$$

$$\text{Swelling ratio} = \frac{W_s - W_a}{W_a}$$

**Tensile test.** Tensile testing was carried out using a Testometric M100-1CT machine equipped with a 50 N cell load (LC5). Rectangular cross-linked sheets were used to perform the measurements, obtained according to the procedure described above. A gauge length of 8 mm, a pretension of 0.1 N, and a test speed of 10 mm min$^{-1}$ were used as parameters for the machine. The tests were performed at room temperature. Young's modulus, elongation at break, and the ultimate strength were determined as averages of five independent drawing experiments performed under the same conditions.

**Compression test.** Compression testing was carried out using a Testometric M100-1CT equipped with a 50 N cell load (LC5) and CPS150 square compression platens. Crosslinked networks were transformed into cylinders with a diameter of 7.5 mm and a height of 3 mm. A preload force of 0.1 N was set, and each test was carried out at a compression speed of 1 mm min$^{-1}$ at room temperature. Young's modulus, compression at break, and the ultimate strength were determined as averages of three experiments performed under the same conditions.

**3D printing.** 3D printing was performed using a custom DLP 3D printer, MONO3-2K40 (Monoprinter). The projector resolution was 1902 × 1080 pixels, with an in-plane resolution of 15 μm. Each layer thickness was 50 μm, with exposure times of 20 s for the first two base layers and 10 s for all subsequent layers. A light intensity of 22 mW cm$^{-2}$ at 405 nm (measured on the surface of the tank) was used for all the printings at room temperature. The porous lattice cube 3D model was generated using the software MSLattice.[23] The resin composition includes 50 wt% poly(valerolactone-*co*-caprolactone)-CA, 49 wt% HEA, 1 wt% PETA, 1 wt% BAPO, 0.05 wt% Sudan I, and 0.1 wt% TEMPO. After printing, the objects were washed with acetone.

**Cell seeding efficiency.** DC2.4 cells, a type of dendritic cell derived from the bone marrow of C57BL/6 mice, were seeded at a density of 5 × 10$^5$ cells per scaffold. After seeding, 1 mL of growth medium was added to each well, and the cells were pre-cultured for 24 hours. Following this incubation, the cell-seeded scaffolds were transferred to a new 24-well plate. Any remaining unattached cells at the bottom of the wells were detached, counted using a hemocytometer, and recorded.

**Cellular metabolic activity assay.** To determine the cell metabolic activity and viability on the scaffolds, an Alamar Blue assay was performed on the scaffolds. The metabolic activity of the DC2.4 cells in the scaffolds was assessed on days 1, 3 and 7, using an Alamar Blue assay (Biosciences) according to the manufacturer's instructions. Growth media (which consisted of high-glucose Dulbecco's modified Eagle medium (DMEM) (Sigma-Aldrich) supplemented with 10% (v/v) fetal bovine serum (FBS) (ThermoFisher Scientific), 0.002% (v/v) primocin (ThermoFisher Scientific), 1% (v/v) GlutaMAX (ThermoFisher Scientific), and 1% (v/v) non-essential amino acids (ThermoFisher Scientific)) containing 10% Alamar Blue was added at 37 °C for 2 hours. A spectrophotometer (Wallac 1420 Victor2 D) with an excitation wavelength of 550 nm and an emission wavelength of 590 nm was used to measure the resulting fluorescence levels. Chondrogenic media containing 10% Alamar Blue was used as a blank sample, and its fluorescence reading was subtracted from the experimental readings to eliminate background fluorescence.

**DNA survey of cell activities.** For DNA content analysis within the scaffolds, Invitrogen™ Quant-iTTM PicoGreen™ assays (Fisher Scientific) were used as per the manufacturer's instructions. Scaffolds were removed from the media and washed in PBS. The scaffolds were then submerged in 500 μL of lysis buffer (0.2 M carbonate and 1% Triton X100) in an Eppendorf tube. Samples were subjected to three freeze–thaw cycles to achieve complete cell lysis before analysis. 100 μL of each sample was then transferred to a black 96-well plate along with 100 μL of PicoGreenTM reagent. The fluorescence was recorded at 538 nm, and the final DNA concentration was calculated from a standard curve generated using standards formulated according to the manufacturer's instructions.

## Results and discussion

### Synthesis of poly(caprolactone -*co*-valerolactone)-cinnamic acid

A four-arm poly(valerolactone-*co*-caprolactone) end-functionalised with cinnamic acid (P(CL-*co*-VL)-CA) was first synthesised. A 3 : 2 molar copolymer composition (CL : VL) was selected for its amorphous, viscous liquid nature at room temperature, eliminating the need for solvents during 3D printing. To align with increasing sustainability demands in polymer synthesis, the preparation of P(CL-*co*-VL)-CA was optimised into a one-pot, solvent-free, and work-up-free process (Fig. 2). In the first step, CL and VL were copolymerised in bulk *via* tin(II) octoate-catalysed ring-opening polymerisation in the presence of pentaerythritol. A monomer to initiator ratio (CL + VL to OH groups) of 5 was applied for a theoretical

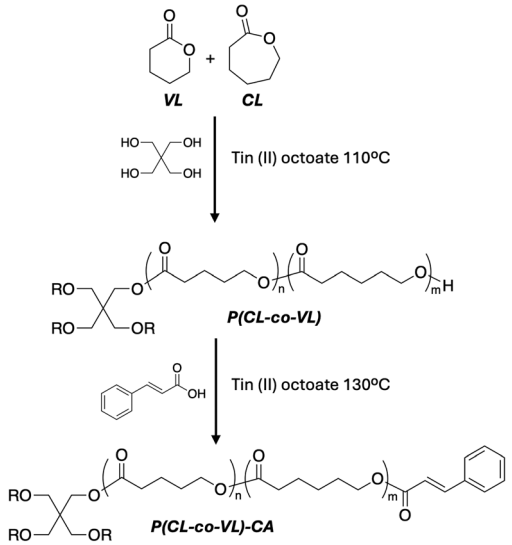


**Fig. 2** Solvent-free synthesis of photo-curable P(CL-*co*-VL)-CA.

$M_n$ of 555 per arm or 2240 g mol$^{-1}$ for the four arm copolyester. Once the copolymerisation reached >96% monomer conversion, determined by the near-complete disappearance of the monomer $^1$H NMR signals corresponding to ε-caprolactone and δ-valerolactone (4.20–4.35 ppm; Fig. S1), CA was added directly to the reaction, facilitating esterification with the terminal hydroxyl groups of P(CL-*co*-VL). The final copolymer was recovered as a viscous yellowish liquid without workup (Fig. S5). This approach eliminates the need for the typically used cinnamoyl chloride as an end-capping reagent,[24] as well as the use of solvents. End-capping was confirmed by the appearance of the doublet at 7.67 ppm, corresponding to the protons of the CA (Fig. 3), clearly distinguishable from the same protons of the free CA at 7.76 ppm in the $^1$H NMR (Fig. S2). The DOSY NMR of the final P(CL-*co*-VL)-CA displays only one species with no detectable free CA (Fig. S3). Finally, size exclusion chromatography (SEC) traces of P(CL-*co*-VL) and P(CL-*co*-VL)-CA showed a small increase in the molecular weight after CA addition, in line with expectations for end-capping (Fig. S4). The resulting P(CL-*co*-VL)-CA was used directly in subsequent studies without purification.

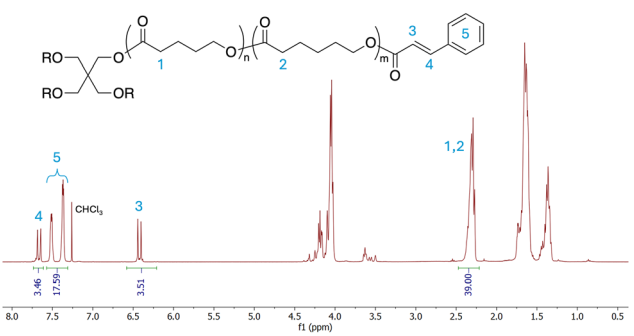


**Fig. 3** $^1$H NMR spectrum of P(CL-*co*-VL)-CA ($CDCl_3$).

## Preparation of single and double crosslinked networks

To design a network with time-dependent crosslinking, it is essential to understand the photoreactivity of both acrylate and cinnamic acid. Three resin formulations were therefore prepared containing P(CL-*co*-VL)-CA or HEA, and a formulation containing a 1 : 1 (wt/wt) mixture of P(CL-*co*-VL)-CA and HEA (Table S1). For the HEA-containing formulations, 1 wt% pentaerythritol tetraacrylate (PETA) was added as a crosslinker. All formulations contained 1 wt% BAPO photoinitiator to ensure comparison.

Photorheology was first performed under 405 nm irradiation at 9 mW cm$^{-2}$. As shown in Fig. 4A, both HEA and the P(CL-*co*-VL)-CA/HEA blends exhibited rapid polymerisation, with a distinct gel point at 5 s. In contrast, P(CL-*co*-VL)-CA alone showed no measurable polymerisation after 5 min of exposure at 405 nm. While the blend displayed similar gelation kinetics to pure HEA, its lower plateau modulus reflects the reduced crosslink density arising from the non-crosslinking copolyester component. The absence of cinnamate photodimerisation at 405 nm suggests that the two crosslinking processes, HEA radical polymerisation and CA dimerization, can be temporally separated. This is in agreement with a CA/acrylate hydrogel system we previously reported.[25] To further verify this behaviour, the photokinetics of CA in the P(CL-*co*-VL)-CA/HEA resin were monitored by FTIR. The films were first irradiated at 405 nm for 2 min to allow the formation of the HEA network. The HEA C═C band at 1619 cm$^{-1}$ disappeared com-

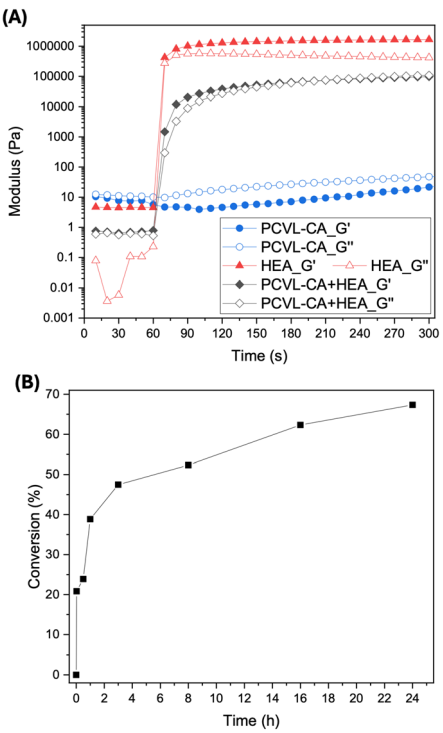


**Fig. 4** (A) Photo rheology study of P(CL-*co*-VL)-CA, HEA and P(CL-*co*-VL)-CA/HEA resins, with irradiation started at 60 s (405 nm, 9 mW cm$^{-2}$); (B) plots of CA conversion from P(CL-*co*-VL)-CA/HEA resin after exposure to 365 nm UV light determined by FTIR through deconvolution of the C═C related peaks.

pletely within this time, confirming efficient acrylate polymerisation. A small degree of cinnamic acid double-bond conversion was also observed by FTIR during this exposure at 405 nm. This expected reactivity is explained by the addition of propagating poly(HEA) radicals to the cinnamate system, resulting in copolymerization/grafting rather than the formation of a distinct cinnamate-crosslinked network. Cinnamate conversion, leading to a cinnamate network, proceeded only under prolonged 365 nm exposure (9 mW $cm^{-2}$), reaching ~67% after 24 h, which is in agreement with systems reported in the literature (Fig. 4B).[26,27] Together, these results demonstrate that P(CL-*co*-VL)-CA/HEA resins can be crosslinked *via* rapid acrylate polymerisation while preserving most cinnamate functionality for controlled, delayed formation of a second network during post-printing UV treatment.

### Gel and mechanical properties of single and double crosslinked networks

Based on the distinct photoreactivities of P(CL-*co*-VL)-CA and HEA, we investigated whether the mechanical properties of the P(CL-*co*-VL)-CA/HEA networks could be altered by controlling the irradiation time. Tensile testing was therefore performed on all networks to assess differences in modulus and stress–strain behaviour. As a reference, the P(CL-*co*-VL)-CA network was first characterised after 24 h of UV irradiation at 365 nm, yielding an elastic modulus of 1.5 ± 0.8 MPa and a strain of 15.6 ± 3.7% – a quite brittle material that is difficult to handle. For the P(CL-*co*-VL)-CA/HEA blend irradiated for only 2 min at 405 nm, a markedly lower modulus (0.29 MPa) and a higher strain (~45%) were observed, consistent with the presence of non-crosslinked polyester chains. To map the evolution of mechanical performance, additional samples were irradiated for 0.5, 1, 3, 8, 16, and 24 h at 365 nm (Fig. 5A). The elastic modulus increased steadily from 0.29 to 1.80 MPa over this period (Fig. 5B), reflecting the progressive photodimerisation of cinnamate groups. The elongation at break also increased alongside the ultimate strength (Fig. 5A and Fig. S7), indicating that the two networks, acrylate and polyester, remain mostly independent rather than forming a single, densely crosslinked structure.

The compressive behaviour of the crosslinked networks was evaluated through uniaxial compression testing. Due to minor surface imperfections or slight misalignment at the initial contact, the compressive modulus was determined from the linear region between 20% and 30% strain, rather than the initial portion of the stress–strain curve. The compressive modulus increased progressively with longer light exposure times (Fig. 5C), in agreement with the trend observed for the tensile modulus, ranging from 375 kPa to 1445 kPa for the sample with the longest light exposure (Table S4). Notably, none of the samples exhibited a breaking point even at high compressive strains. However, the maximum strain achievable before reaching the instrument's load limit decreased with increasing light exposure time. This indicates that while the gels maintain structural integrity and display highly ductile behaviour under compression, the second crosslinking reduces overall compressibility without leading to failure.

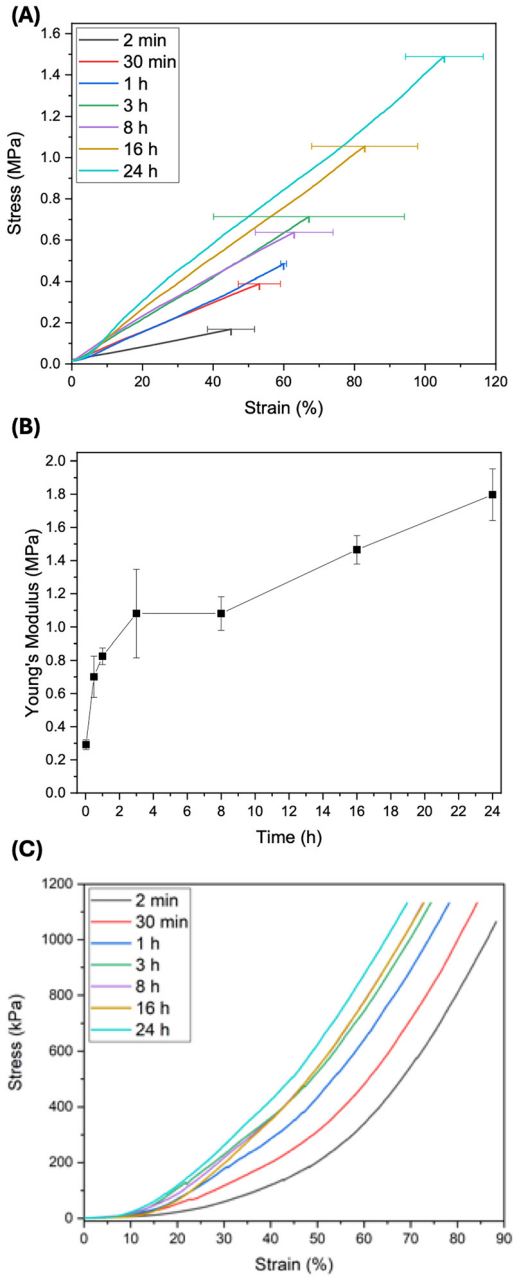


**Fig. 5** (A) Tensile test of P(CL-*co*-VL)-CA/HEA networks at different irradiation times obtained from cast films. (B) Plots of Young's modulus of P(CL-*co*-VL)-CA/HEA as a function of irradiation time. 405 nm was used for the samples at 2 min; all successive samples were irradiated at 365 nm. (C) Compression test of P(CL-*co*-VL)-CA/HEA networks at different irradiation times obtained from cylindrical-shaped samples. Representative curves for each time point shown. No breaking point was detected for any of the samples.

Stress relaxation tests were performed to evaluate the viscoelastic response of the networks under constant strain (Fig. S8). All samples exhibited an initial rapid decay in relaxation modulus followed by a slower levelling towards a plateau after 10 seconds, characteristic of viscoelastic networks. However, a strong dependence on the irradiation time was

observed. The gel crosslinked for 2 min (corresponding to the formation of the first polyHEA network) showed a low initial modulus and relaxed almost completely to near-zero values within seconds to minutes. As crosslinking time increased to 1 h and 8 h, the initial relaxation modulus increased, with a slightly slower decay. The most pronounced effect appeared in the 24 h crosslinked sample, which exhibited a significantly higher initial relaxation modulus and a much slower relaxation profile, retaining a clear non-zero equilibrium modulus plateau (~200 Pa) even after 1000 s. This trend indicates that increasing crosslinking density due to the second network enhances the elastic character of the gel network.

To corroborate that the mechanical changes arise from the gradual conversion of P(CL-*co*-VL)-CA, gel fraction measurements were performed on samples irradiated for 2 min and 24 h. The 2 min network exhibited a gel fraction of around 51%, consistent with primary polymerisation of the acrylate component, with minor incorporation of cinnamic acid along polyHEA chains as discussed above. After 24 h of irradiation, the gel fraction increased to around 80%, corresponding to approximately 60% cinnamate conversion (Table S3). At the same time, the swelling ratio of the networks halved from 2 min to 24 h curing time (136 *vs.* 69%). These data confirm the hypothesis that the modulus of the polymer networks can be tuned by varying the UV exposure time during photopolymerization. Furthermore, they demonstrate that the two constituent networks form mostly independently, with crosslinking occurring at distinct temporal stages under controlled irradiation conditions.

Degradation tests were conducted in a 0.2 M NaOH aqueous solution at 37 °C using samples irradiated at 365 nm for 24 h. The gel fraction decreased progressively from ~98% to ~55% within 120 h and remained approximately constant up to 168 h (Fig. S9). This trend indicates that degradation predominantly affects the polyester component of the network, while the polyHEA fraction remains largely unaffected under these conditions. This is consistent with the susceptibility of polyesters to hydrolytic cleavage in aqueous environments, in contrast to the relative stability of polyacrylates. At the same time, the swelling ratio increased substantially, increasing from ~500–600% at early time points to ~6500–7000%, reflecting enhanced water uptake as the crosslink density decreases during selective polyester degradation.

### 3D printing of CA/HEA networks

The printability of the P(CL-*co*-VL)-CA/HEA resin using a digital light processing (DLP) printer was investigated. The resin formulation (HEA : P(CL-*co*-VL)-CA : PETA : BAPO = 49 : 49 : 1 : 1 by weight %) was printed layer-by-layer (50 μm per layer) under 405 nm irradiation for 10 s at 22 mW $cm^{-2}$, with the addition of Sudan I as a photo-absorber (0.05 wt%) and TEMPO (0.1 wt%) as a radical scavenger. To assess printing accuracy, a "HEISE GROUP" 2.5D test object (10 mm × 10 mm × 1.5 mm) was first fabricated (Fig. 6A). Dimensional deviations of <2% were observed in both the *X* and *Y* directions compared to the CAD model, demonstrating excellent resolution. To further validate suitability for more advanced 3D scaffold a more complex design (10 mm × 10 mm × 10.2 mm) was printed at a speed of 2.5 mm $h^{-1}$ (Fig. 6B–D). The scaffold exhibited well-defined pores (2.2 mm), and the overall dimensional deviation across the *X*, *Y*, and *Z* axes was only 0.5%, confirming high fidelity and structural reproducibility. The formulation exhibited good print resolution, attributed to the selective photopolymerisation and crosslinking of HEA, which is well established to have superior printability.[28,29] Consequently, the presence of HEA enabled effective printing of the entire resin mixture, despite the slower nature of P(CL-*co*-VL)-CA.

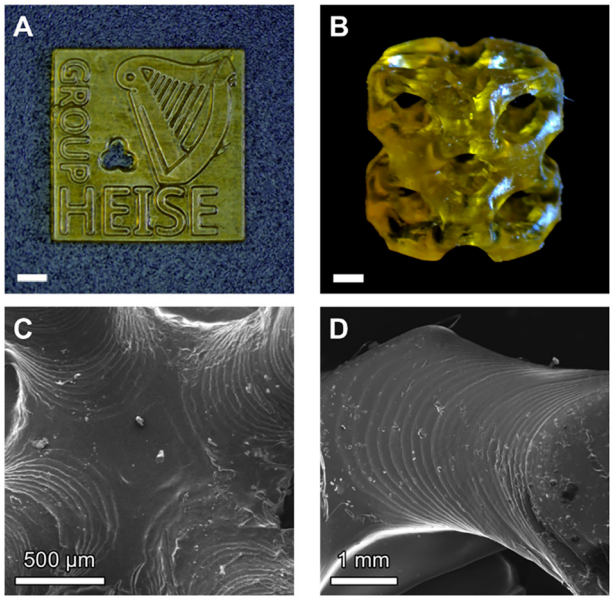


**Fig. 6** (A) Photograph of the 2.5 D printed P(CL-*co*-VL)-CA/HEA resin (scale bar 1.5 mm). (B) Photograph of the 3D-printed object from the P(CL-*co*-VL)-CA/HEA resin (scale bar 1.5 mm). (C and D) SEM images of the object displayed in B. For CAD 3D models see Fig. S10.

Given the resin's time-dependent crosslinking behaviour, it was then examined whether printed structures retained the tuneable mechanical properties demonstrated in cast films. Rectangular specimens (*L*20 mm × *W*10 mm × *H*0.5 mm) were printed under the same exposure conditions as the 3D scaffold. Immediately after printing, the samples exhibited a modulus of 0.34 ± 0.04 MPa and an elongation at break of 30.7 ± 5.9% (Fig. 7), values comparable to the ones obtained from the 2 min irradiated cast samples. A second batch of printed specimens was then post-irradiated for 24 h at 365 nm (9 mW $cm^{-2}$). These samples attained values of 0.8 MPa for Young's modulus and 37% for elongation at break. The observed differences in mechanical properties (*e.g.*, halved elastic modulus in DLP-printed samples compared to cast films) could hypothetically derive from limited diffusion of the cinnamate-functionalized polymer, particularly at the formation of interfaces during layer-by-layer 3D printing.[30] To overcome this, 1 wt% benzophenone was added to the resin formulation as a photosensitizer able to transfer energy to the cinnamate groups, promoting the 2 + 2 photodimerization.[31] These printed films,

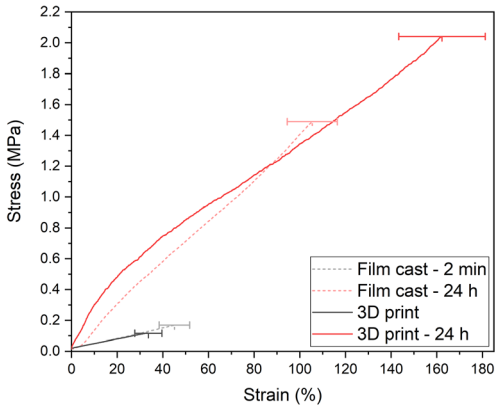


**Fig. 7** Tensile test of P(CL-*co*-VL)-CA/HEA 3D printed networks directly after printing and after 24 h of post-curing. DLP 3D printing conditions: 405 nm, 22 mW $cm^{-2}$, for 10 seconds per layer. Post-curing conditions: 365 nm, 9 mW $cm^{-2}$, for 24 hours.

after 24 h at 365 nm, reached a Young's modulus of 1.79 ± 0.05 MPa, an elongation at break of 164.5 ± 18.9 and a stress at break of 2.1 ± 0.6 MPa. These values are comparable to the ones obtained *via* film casting, showing that the time-dependent properties can be reproduced *via* 3D DLP printing.

### Cell adhesive and activity study of CA/HEA networks

The initial cell seeding efficiency on day 1 (Fig. 8) reflects the proportion of cells that successfully adhered and remained on each scaffold after the seeding process. All three samples exhibited similar behaviour (around 80%) with values comparable within experimental error. After 7 days of culture, a different trend was observed in the DNA content, with a significantly higher value detected on the dual-cured network scaffold compared to the single-cured one. Meanwhile the network made only from P(CL-*co*-VL)-CA exhibited a very low level of cell proliferation, as expected due to the poor wettability and lack of bioactive functional groups of the polyester.[32,33] The higher DNA content observed in the P(CL-*co*-VL)-CA/HEA scaffold likely results from a synergistic balance between hydrophilicity and mechanical stability, which enhances cell adhesion and proliferation.[31] In contrast, the pure poly(HEA) scaffold may be too hydrophilic or too soft, limiting stable cell attachment and growth, although other factors such as the mesh size might also play a role.[34–37]

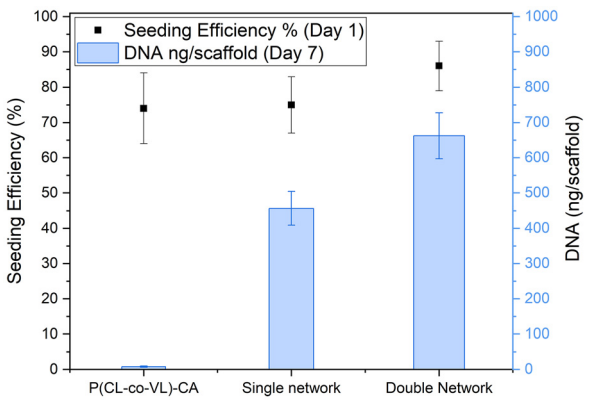


**Fig. 8** Cell seeding efficiency (%) on day 1 (scatter black plot) and the corresponding DNA content (ng/scaffold) on day 7 (blue bars) for three different polymer crosslinked networks after seeding with DC2.4 cells, a type of dendritic cell derived from the bone marrow of C57BL/6 mice. P(CL-*co*-VL)-CA is the network made from P(CL-*co*-VL)-CA only. Single- and double-cured network derived from the P(CL-*co*-VL)-CA/HEA resin irradiated for 2 min at 405 nm (single-cured) and 24 h at 365 nm (double-cured).

## Conclusions

In this work, we reported a DLP-printable hydrogel scaffold with post-printing tuneable mechanical properties. This concept exploits two orthogonal photochemical reactions: rapid free-radical acrylate polymerisation and slower cinnamate photodimerisation. The primary network is formed during printing through the free-radical polymerisation of HEA, while the secondary network is subsequently crosslinked *via* controlled photodimerisation of degradable cinnamic-acid-functionalised P(CL-*co*-VL)-CA. By varying the extent of P(CL-*co*-VL)-CA crosslinking over time, the mechanical properties such as the elastic modulus, compression strength and stress relaxation of the double-network scaffolds could be tuned. Overall, this strategy provides a versatile route to DLP-printed hydrogel scaffolds, combining fast DLP 3D printing with a slower post-printing treatment to allow mechanical properties to be dialled in. This can be achieved from a single resin formulation. While both single- and double-crosslinked P(CL-*co*-VL)-CA/HEA networks supported high levels of cell proliferation, more advanced cell studies with relevant cell lines need to be investigated to elucidate the potential of these materials for tissue engineering applications.

## Author contributions

Bo Li: conceptualisation, writing – original draft, and writing – review and editing. Gianluca Bartolini Torres: investigation, methodology, visualisation, and writing – review and editing. Na Zhoa: investigation. Jonathan J. P. Peters: investigation. Guonan Ji: investigation. Quinten Thijssen: methodology and writing – review and editing. Andreas Heise: supervision, funding acquisition, and writing – review and editing.

## Conflicts of interest

There are no conflicts to declare.

## Data availability

The data supporting this article have been included as part of the supplementary information (SI). Supplementary infor-

mation (SI): methods of polymer characterisation (NMR, FTIR, GPC, DSC, and rheology), additional resin analysis (FTIR, mechanical properties, and swelling), and additional 3D printing data (CAD models and viscosity). See DOI: https://doi.org/10.1039/d6lp00051g.

## Acknowledgements

This project was supported in part by a research grant from the Research Ireland under grant number 12/RC/2073_P2. This publication has emanated from research supported in part by a grant from Research Ireland and the European Regional Development Fund (ERDF) under Grant Number 13/RC/2073_P2. J. J. P. P. acknowledges the Research Ireland grant URF\R\241034 and the TCD Advanced Microscopy Facility. The murine dendritic cell line DC2.4 was kindly provided by Prof. Olga Piskareva (RCSI University of Medicine and Health Sciences).

## References

1 J. P. Vacanti and R. Langer, *Lancet*, 1999, **354**, S32.
2 M. U. A. Khan, M. A. Aslam, M. F. B. Abdullah, A. Hasan, S. A. Shah and G. M. Stojanović, *Mater. Today Chem.*, 2023, **34**, 101818.
3 F. J. O'Brien, *Mater. Today*, 2011, **14**, 88.
4 S. Bose, S. Vahabzadeh and A. Bandyopadhyay, *Mater. Today*, 2013, **16**, 496.
5 W. Li, L. S. Mille, J. A. Robledo, T. Uribe, V. Huerta and Y. S. Zhang, *Adv. Healthcare Mater.*, 2020, **9**, 2000156.
6 X. Yuan, W. Zhu, Z. Yang, N. He, F. Chen, X. Han and K. Zhou, *Adv. Mater.*, 2024, **36**, 2403641.
7 B. Zhang, J. Huang and R. J. Narayan, *J. Mater. Chem. B*, 2020, **8**, 8149.
8 A. Seidi, M. Ramalingam, I. Elloumi-Hannachi, S. Ostrovidov and A. Khademhosseini, *Acta Biomater.*, 2011, **7**, 1441.
9 P. Fu, H. Li, J. Gong, Z. Fan, A. T. Smith, K. Shen, T. O. Khalfalla, H. Huang, X. Qian, J. R. McCutcheon and L. Sun, *Prog. Polym. Sci.*, 2022, **126**, 101506.
10 H. D. Tran, C. Vazquez-Martel, S. O. Catt, Y. Jia, M. Tsotsalas, C. A. Spiegel and E. Blasco, *Adv. Funct. Mater.*, 2024, **34**, 2315238.
11 J. Chen, C. Virrueta, S. Zhang, C. Mao and J. Wang, *Mater. Today*, 2024, **77**, 66.
12 G. Bartolini Torres, S. Stefanovic, B. Li and A. Heise, *ACS Appl. Polym. Mater.*, 2024, **6**, 11241.
13 G. Bartolini Torres, T. Xia, D. Yu, Q. Thijssen, S. Van Vlierberghe, B. Li and A. Heise, *ACS Polym. Au*, 2025, **5**, 956.
14 B. Zhang, K. Kowsari, A. Serjouei, M. L. Dunn and Q. Ge, *Nat. Commun.*, 2018, **9**, 1831.
15 G. Zhu, N. von Coelln, Y. Hou, C. Vazquez-Martel, C. A. Spiegel, P. Tegeder and E. Blasco, *Adv. Mater.*, 2024, **36**, 2401561.
16 Q. Thijssen, A. Quaak, B. Bijleveld, B. Li, L. Van Daele, A. Heise and S. Van Vlierberghe, *Chem. Rev.*, 2026, **126**, 1258.
17 R. Dwivedi, S. Kumar, R. Pandey, A. Mahajan, D. Nandana, D. S. Katti and D. Mehrotra, *J. Oral Biol. Craniofac. Res.*, 2020, **10**, 381.
18 H. Ye, K. Zhang, D. Kai, Z. Li and X. J. Loh, *Chem. Soc. Rev.*, 2018, **47**, 4545.
19 M. Salehabadi and H. Mirzadeh, *Adv. Mater. Technol.*, 2025, **10**, 2401522.
20 I. Engelberg and J. Kohn, *Biomaterials*, 1991, **12**, 292.
21 K. D. Samson, V. Hidalgo-Alvarez, T. R. Dargaville and F. P. Melchels, *Adv. Funct. Mater.*, 2023, **33**, 2213797.
22 G. Damonte, L. Maddalena, A. Fina, D. Cavallo, A. J. Müller, M. R. Caputo, A. Mariani and O. Monticelli, *Eur. Polym. J.*, 2022, **171**, 111226.
23 O. Al-Ketan and R. K. Abu Al-Rub, *Mater. Des. Process. Commun.*, 2021, **3**, e205.
24 K. Luo, L. Wang, M.-X. Wang, R. Du, L. Tang, K.-K. Yang and Y.-Z. Wang, *ACS Appl. Mater. Interfaces*, 2023, **15**, 44373.
25 G. Ji, S. An, G. B. Torres, F. J. O'Brien, Z. Song, B. Li and A. Heise, *Polym. Chem.*, 2026, **17**, 207.
26 S. Colanges, K. Ballu, A. Lamouroux, G. Pecastaings, I. Ly, C. Le Coz, T. Tassaing, T. Brunet, E. Grau, H. Cramail, O. Mondain-Monval and T. Vidil, *Eur. Polym. J.*, 2025, **223**, 113655.
27 D. Tunc, C. Le Coz, M. Alexandre, P. Desbois, P. Lecomte and S. Carlotti, *Macromolecules*, 2014, **47**, 8247.
28 F. Shen, C. Tang, Y. Yang, G. Qin, M. Li, H. Jiang, M. Wu and S. Chen, *Molecules*, 2025, **30**, 4000.
29 F. Chen, R. Li, J. Sun, G. Lu, J. Wang, B. Wu, J. Li, J. Nie and X. Zhu, *J. Appl. Polym. Sci.*, 2021, **138**, e49965.
30 H. Gojzewski, Z. Guo, W. Grzelachowska, M. G. Ridwan, M. A. Hempenius, D. W. Grijpma and G. J. Vancso, *ACS Appl. Mater. Interfaces*, 2020, **12**, 8908.
31 S. Poplata, A. Tröster, Y.-Q. Zou and T. Bach, *Chem. Rev.*, 2016, **116**, 9748.
32 M. Chen, Z. Feng, W. Guo, D. Yang, S. Gao, Y. Li, S. Shen, Z. Yuan, B. Huang, Y. Zhang, M. Wang, X. Li, L. Hao, J. Peng, S. Liu, Y. Zhou and Q. Guo, *ACS Appl. Mater. Interfaces*, 2019, **11**, 41626.
33 R. Singh, D. Eitler, R. Morelle, R. P. Friedrich, B. Dietel, C. Alexiou, A. R. Boccaccini, L. Liverani and I. Cicha, *Eur. Polym. J.*, 2020, **134**, 109838.
34 J. Lee, B. Song, R. Subbiah, J. J. Chung, U. H. Choi, K. Park, S.-H. Kim and S. J. Oh, *Sci. Rep.*, 2019, **9**, 2463.
35 A. A. Solbu, D. Caballero, S. Damigos, S. C. Kundu, R. L. Reis, Ø. Halaas, A. S. Chahal and B. L. Strand, *Mater. Today Bio*, 2023, **18**, 100537.
36 H. Y. Yoshikawa, F. F. Rossetti, S. Kaufmann, T. Kaindl, J. Madsen, U. Engel, A. L. Lewis, S. P. Armes and M. Tanaka, *J. Am. Chem. Soc.*, 2011, **133**, 1367.
37 S. Nishimura, T. Yoshida, N. Higashi and T. Koga, *Adv. Mater. Technol.*, 2024, **9**, 2301598.